




Article

Evaluation of Structural and Optical Properties of Graphene Oxide-Polyvinyl Alcohol Thin Film and Its Potential for Pesticide Detection Using an Optical Method

Nurul Illya Muhamad Fauzi ¹, Yap Wing Fen ^{1,2,*} , Jaafar Abdullah ^{1,2} , Mazliana Ahmad Kamarudin ², Nur Alia Sheh Omar ², Faten Bashar Kamal Eddin ² , Nur Syahira Md Ramdzan ² and Wan Mohd Ebtisyam Mustaqim Mohd Daniyal ¹

- ¹ Functional Nanotechnology Devices Laboratory, Institute of Nanoscience and Nanotechnology, Universiti Putra Malaysia (UPM), Serdang 43400, Selangor, Malaysia; gs55644@student.upm.edu.my (N.I.M.F.); jafar@upm.edu.my (J.A.); gs50207@student.upm.edu.my (W.M.E.M.M.D.)
- ² Faculty of Science, Universiti Putra Malaysia (UPM), Serdang 43400, Selangor, Malaysia; mazliana_ak@upm.edu.my (M.A.K.); nuralia_so@upm.edu.my (N.A.S.O.); gs51801@student.upm.edu.my (F.B.K.E.); gs52842@student.upm.edu.my (N.S.M.R.)
- * Correspondence: yapwingfen@upm.edu.my

Abstract: In the present work, graphene oxide (GO)–polyvinyl alcohol (PVA) composites thin film has been successfully synthesized and prepared by spin coating techniques. Then, the properties and morphology of the samples were characterized using Fourier transform infrared spectroscopy (FTIR), ultraviolet-visible spectroscopy (UV-Vis), and atomic force microscopy (AFM). Experimental FTIR results for GO–PVA thin film demonstrated the existence of important functional groups such as $-\text{CH}_2$ stretching, $\text{C}=\text{O}$ stretching, and $\text{O}-\text{H}$ stretching. Furthermore, UV-Vis analysis indicated that the GO–PVA thin film had the highest absorbance that can be observed at wavelengths ranging from 200 to 500 nm with a band gap of 4.082 eV. The surface morphology of the GO–PVA thin film indicated the thickness increased when in contact with carbaryl. The incorporation of the GO–PVA thin film with an optical method based on the surface plasmon resonance (SPR) phenomenon demonstrated a positive response for the detection of carbaryl pesticide as low as 0.02 ppb. This study has successfully proposed that the GO–PVA thin film has high potential as a polymer nanomaterial-based SPR sensor for pesticide detection.

Keywords: graphene oxide; polyvinyl alcohol; structural properties; optical properties; surface plasmon resonance



Citation: Fauzi, N.I.M.; Fen, Y.W.; Abdullah, J.; Kamarudin, M.A.; Omar, N.A.S.; Eddin, F.B.K.; Ramdzan, N.S.M.; Daniyal, W.M.E.M.M. Evaluation of Structural and Optical Properties of Graphene Oxide-Polyvinyl Alcohol Thin Film and Its Potential for Pesticide Detection Using an Optical Method. *Photonics* **2022**, *9*, 300. <https://doi.org/10.3390/photonics9050300>

Received: 30 March 2022

Accepted: 17 April 2022

Published: 28 April 2022

Publisher's Note: MDPI stays neutral with regard to jurisdictional claims in published maps and institutional affiliations.



Copyright: © 2022 by the authors. Licensee MDPI, Basel, Switzerland. This article is an open access article distributed under the terms and conditions of the Creative Commons Attribution (CC BY) license (<https://creativecommons.org/licenses/by/4.0/>).

1. Introduction

Sensors are becoming increasingly vital and have already dominated in everyday life. This is due to the fact that sensors provide numerous advantages such as improved medical diagnostics, health and safety, environmental monitoring, security for people, and the performance of energy sources [1–10]. Therefore, the selective identification of materials and methods is an important issue in the development of sensor technology to ensure that the sensor is adequately sensitive. In the past few decades, graphene oxide (GO) is one of the suitable nanoparticles that have received copious attention as a modish class of substance owing to its promising features in sensor application. GO contains functional groups such as carboxyl, epoxy, carbonyl, and hydroxyl [11–20], which possess special features such as the ability to disperse well in a wide range of polymers and organic solvents [21–30]. These properties mean that GO can be applied in nanoelectronics [31,32], catalysis [33–39], nanocomposites [40,41], sensor technology [42–44], water purification [45–53], and drug delivery [54–61]. However, to improve the properties of GO and increase its effectiveness in the field of sensor applications, GO needs to be modified with other materials. According

to prior research, the composite materials employed for GO modification are metal, metal oxide, polymer, organic matter, and bio-composite materials (enzyme and antibody) [62–74]. This combination has been demonstrated to have a positive interaction within the various applications [75–77].

Recently, graphene oxide-based polymer composites have been shown to be the most interesting research area. The polymer which is composed of macromolecules has been reported to be used in a wide variety of sensor designs and applications due to its promising potential [78–91]. Additionally, this combination has been reported as an effective approach for achieving extraordinary performance and creating new functionalities in diverse applications due to its distinct shape, high surface area, and tiny size [92–94]. One of the polymers that are widely employed in a variety of applications is polyvinyl alcohol (PVA). This is due to its availability, dielectric strength, promising optical properties, being water-soluble, hydroxyl-rich, and bio-degradable [95–102]. Typically, polymer-graphene composites containing graphene oxide (GO) or graphene platelets were synthesized through exfoliation in the organic solvent [103–108]. In the matter of water-soluble polymers like PVA, GO would be the best choice due to its high amount of oxygenated groups making it hydrophilic and easily dispersed in water [31]. Another advantage is because of its high aspect ratio, meaning the large lateral size of sheets and minimal thicknesses [109]. Homogenous dispersion of GO in the PVA matrix at the molecule level can also enhance the properties of the mechanical characteristics, electrical conductivity, and thermal stability of the nanocomposites [110–115]. Inspired by preceding work, GO–PVA has been extensively reported to be an excellent material for memory devices, radiofrequency, bone tissue engineering applications, and humidity sensors [116–127]. Importantly, GO–PVA also offers simple implementation, it is economical, harmless, non-toxic, and easily degradable.

However, the characterization of this composite material-based thin film is rarely investigated, and the integration of PVA with low-concentration GO is not reported. Therefore, it is of interest to investigate further the structural and optical properties of this excellent composite thin film. To the best of our knowledge, the use of this material as a sensing element in an optical method for pesticide detection has not yet been reported. Surface plasmon resonance (SPR) spectroscopy is one of the powerful and label-free optical methods with high sensitivity [128–134]. This SPR approach is gaining interest among scientists in a wide range of analytical tools for tracing hazardous chemicals [135–142]. Prism coupler and a gold film are normally used to excite surface plasmon. To further increase the sensitivity of SPR, various active layers have been developed on the gold film [143–148]. In this study, the properties of GO–PVA thin film have been investigated and incorporation with SPR attempted for a potential sensing application in pesticide detection.

2. Experimental

2.1. Chemicals

PVA (87–89% hydrolyzed) and carbaryl stock solution 100 mg/mL (98%) were purchased from 3050 Spruce Street Saint Louis, MO 63103 USA. Graphene oxide (4.0 wt%) was purchased from Graphanea in Spain.

2.2. Preparation of GO–PVA and Pesticide Solution

PVA solution was prepared by dissolving 2.0 g of medium molecular weight PVA powder in 36 mL of deionized water and was stirred by a magnetic stirrer at 90 °C for 1 h. After that, GO (0.5 wt%) 5.0 mL was produced by diluting the stock solution (4.0 wt%) with deionized water. To produce the GO–PVA solution, 1.0 mL GO was added with 0.9 mL PVA and ultrasonicated for 30 min at room temperature. A series of standard solutions of 0.02 to 0.06 ppb of carbaryl pesticide were prepared by diluting the stock solution (100 mg/mL) with deionized water. In this preparation, the dilution formula $M_1V_1 = M_2V_2$ was used where M_1 is the concentration of the starting solution and V_1 is the volume of the starting solution. Meanwhile, M_2 is the concentration of the final solution, and V_2 is the volume of the final solution.

2.3. Deposition of Thin Films

Firstly, a thin layer of gold was deposited on a glass slip ($24\text{ mm} \times 24\text{ mm} \times 0.1\text{ mm}$, Menzel-Glaser, Braunschweig, Germany) using a SC7640 sputter coater. The coating process was continued by dropping 0.5 mL of GO–PVA solution on a gold-coated glass slip. To produce GO–PVA composite thin film, a specialty coating system, P-6708D (Inc. Medical Devices, Indianapolis, IN, USA) was used. In this process, the glass slip was spun for 30 s at 3000 rev min. Figure 1 shows the schematic of preparing gold and sensing layer on thin film.

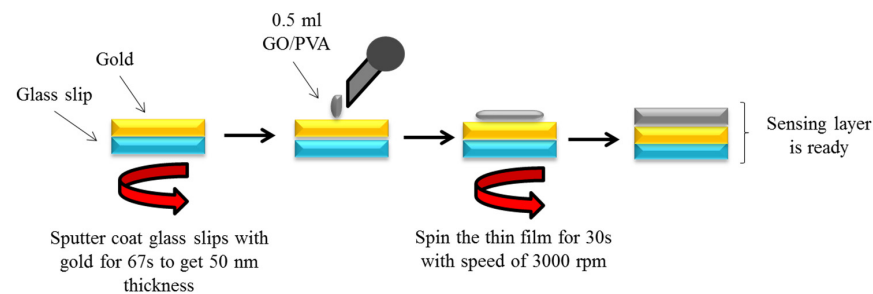


Figure 1. Schematic of preparing gold and sensing layer on thin film.

2.4. Characterization and Potential Sensing

To identify the chemical properties of GO–PVA thin film, Fourier transform infrared spectroscopy (FTIR) was performed using a FTIR spectrophotometer ALPHA Bruker with a wavelength range of $580\text{--}4000\text{ cm}^{-1}$. To determine the absorbance of the sample, UV–Vis–NIR spectroscopy (UV-3600 Shimadzu) was used and measured in the range of 230–500 nm. Then the optical band gap energy can be calculated using the absorption peak or maximum wavelength recorded. Bruker AFM multimode 8 (Quesant, CA, USA) was used to measure and observe the high topography of GO–PVA thin film in the range of $2\text{ }\mu\text{m} \times 2\text{ }\mu\text{m}$. To evaluate the potential sensing of the thin film, an optical instrument based on an SPR Kretschmann configuration was developed, as depicted in Figure 2 [149–154]. In this system, p-polarized light from the source of the He–Ne laser was directly focused on the prism that was attached to the GO–PVA thin film. Then, carbaryl pesticides at concentrations ranging from 0.02 ppb to 0.06 ppb were introduced into the SPR hollow under optimized experimental conditions. After that, the reflected beam was detected by a large area photodiode and subsequently processed by the lock-amplifier (SR 530) to produce the reflectance data.

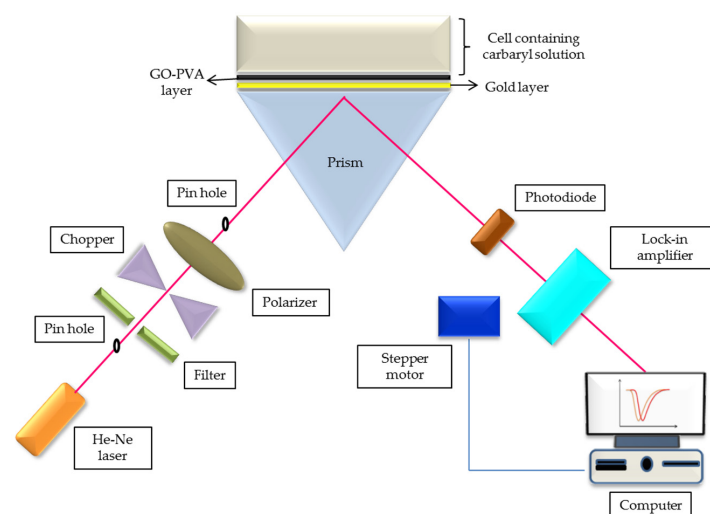


Figure 2. Set-up of surface plasmon resonance (SPR) instrument for sensing performance of the graphene oxide-polyvinyl alcohol (GO–PVA) thin film.

3. Results

3.1. Structural Properties

To further observe the chemical structural properties of GO–PVA thin film, Fourier transform infrared spectroscopy (FTIR) appeared to be the preferred technique for studying the chemical structure. As shown in Figure 3, the FTIR characterizations for GO, PVA, and GO–PVA thin films were carried out at wavenumber ranging from 4000 to 560 cm^{-1} .

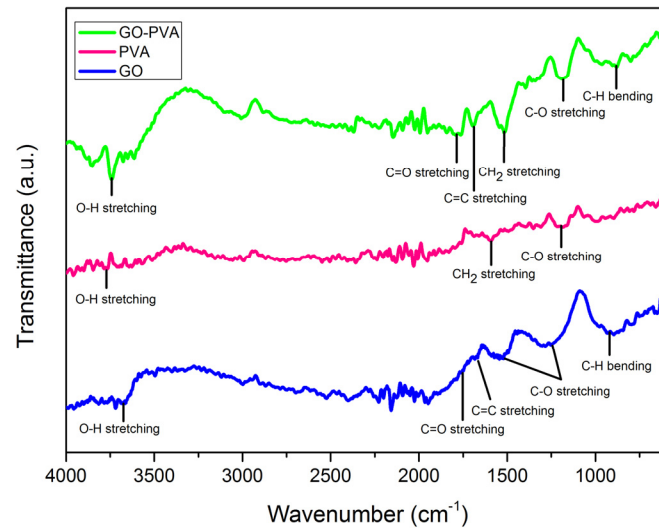


Figure 3. Fourier transform infrared spectroscopy (FTIR) spectra of GO, PVA, and GO–PVA thin film.

According to the FTIR spectra, GO shows the structure can be simplistically assumed in the form of O–H stretching at 3673.81 cm^{-1} , C=O carboxyl stretching at 1750.02 cm^{-1} , C=C stretching at 1664.93 cm^{-1} , C–O epoxy group stretching at 1664.93 cm^{-1} , C–O alkoxy group stretching at 1249.39 cm^{-1} , and C–H bending at 901.22 cm^{-1} , respectively. This analysis is in good correlation with previous studies of GO [155]. Upon examining the PVA spectra, the width at 3771.67 cm^{-1} corresponded to the O–H stretching vibration, the peaks at 1591.18 cm^{-1} and 1194.79 cm^{-1} were due to $-\text{CH}_2$ rocking symmetrical stretching, and the crystalline sequence of PVA on C–O stretching vibration. This finding is in good agreement with the result reported by Lizu et al. (2021) [111]. With the incorporation of GO with PVA, the FTIR spectra indicated the formation of common properties such as O–H, C=O, C=C, $-\text{CH}_2$, C–O stretching, and C–H bending at 3741.18 cm^{-1} , 1774.84 cm^{-1} , 1689.04 cm^{-1} , 1511.76 cm^{-1} , 1182.03 cm^{-1} , and 882.79 cm^{-1} , respectively. It can be seen that the peak became more clear at C=O stretching and C=C stretching compared to the GO single element. The same goes for the $-\text{CH}_2$ stretching, C–O stretching, and O–H stretching compared to the PVA single element. Therefore, these results have proved the existence of chemical interactions on GO and PVA.

3.2. Optical Properties

The optical properties of GO, PVA, and GO–PVA thin films can be evaluated through the UV-Vis results obtained in Figure 4. It can be seen that all thin films have different absorption values at a wavelength of 200 to 500 nm. Clearly, the absorption value on GO–PVA composites thin film is high compared to GO and PVA in single layers. The highest absorption wavelength was between 260 and 300 nm. The absorption peak of approximately 300 nm corresponded to $\pi \rightarrow \pi^*$ transitions of C=O.

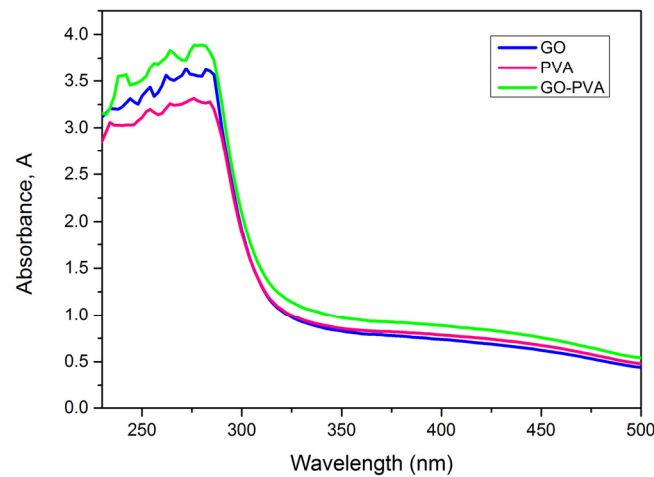


Figure 4. UV-Vis absorbance spectrum of GO, PVA, and GO-PVA thin film.

The absorbance data can be used to interpret information relating to the optical energy band gap of polymer nanocomposites. Then, Beer Lambert’s formula is used to calculate the absorbance coefficient [156]:

$$\alpha = 2.303 \frac{A}{t} \tag{1}$$

where t is the sample’s thickness in m and A is the absorbance value. Followed by the Tauc equation to evaluate the absorbance coefficient and optical band gap [156]:

$$\alpha = \frac{k(h\nu - E_g)^{\frac{1}{2}}}{h\nu} \tag{2}$$

where $h\nu$ represents the photon energy, h is the Plank’s constant, E_g is the optical band gap, and $k = \text{constant value}$. A rearrangement of Equation (2) becomes:

$$(\alpha h\nu)^2 = k(h\nu - E_g) \tag{3}$$

Then the band gap E_g of the GO, PVA, and GO-PVA thin films, was estimated by plotting the $(\alpha h\nu)^2$ against $h\nu$ as presented in Figures 5–7.

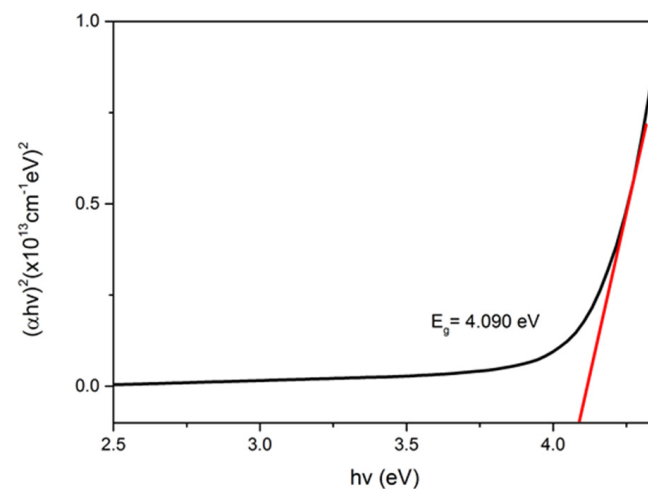


Figure 5. Optical band gap of GO thin film.

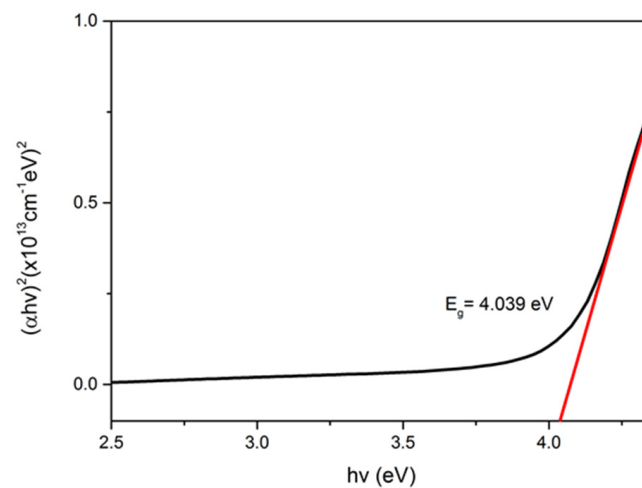


Figure 6. Optical band gap of PVA thin film.

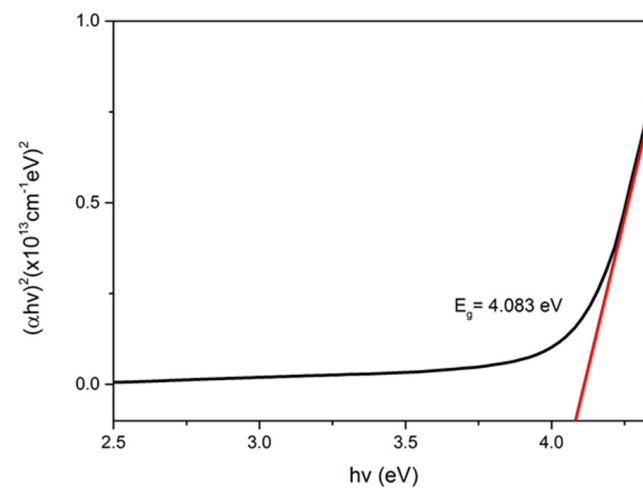


Figure 7. Optical band gap of GO-PVA thin film.

It is shown that the data produced for the optical band gap was different for each component. The highest band gap of 4.090 eV was obtained for GO thin film and the lowest of 4.039 eV was obtained for PVA thin film. The incorporation of GO and PVA gave the band gap value of 4.083 eV.

3.3. Surface Morphology

The microscopic characteristics of GO, PVA, and GO-PVA thin films were visualized well using atomic force microscopy (AFM) in tapping mode. These topographic parameters are measured using the root mean square (RMS) of surface roughness, which shows the relative roughness and the standard deviation of the surface height. In this investigation, the AFM images depict the topography of the composite materials on the gold thin film at a scan size of $2 \mu\text{m} \times 2 \mu\text{m}$ in two-dimensional (2D) and three-dimensional (3D). Figures 8a–c and 9a–c illustrated the 2D and 3D images of GO, PVA, and GO-PVA thin films, respectively. Meanwhile, the AFM result of GO-PVA thin film after being in contact with the carbaryl solution is demonstrated in Figures 8d and 9d.

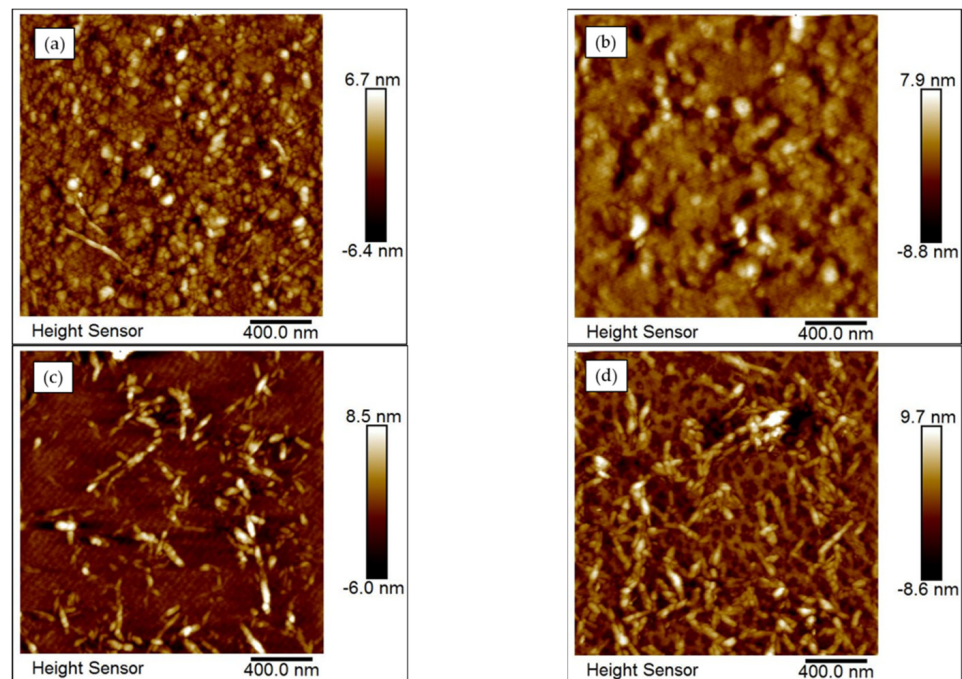


Figure 8. The 2D AFM images: (a) GO, (b) PVA, (c) GO–PVA thin films, and (d) GO–PVA thin film in contact with carbaryl.

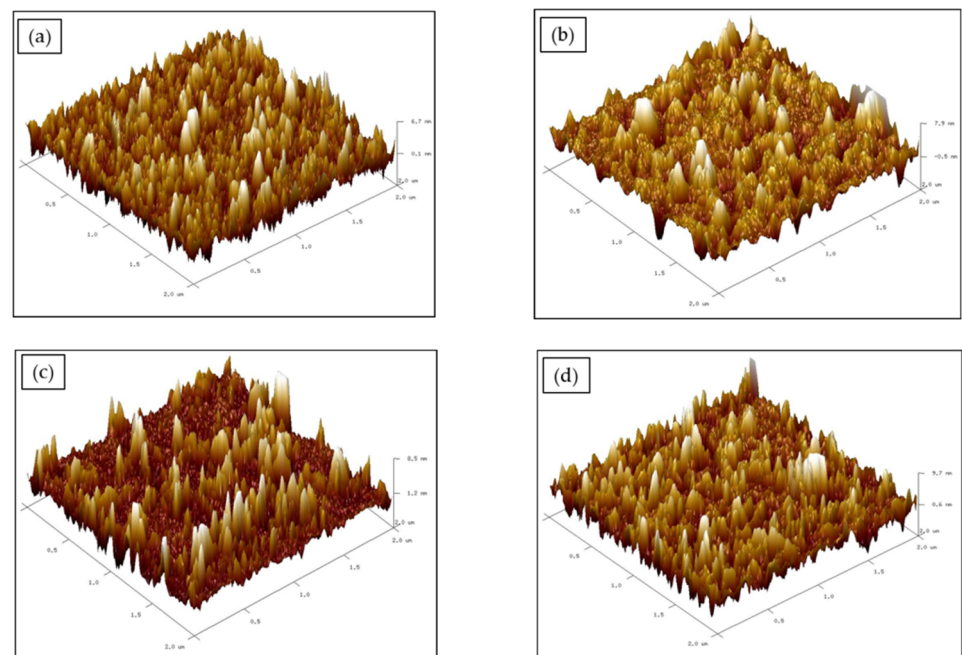


Figure 9. The 3D AFM images: (a) GO, (b) PVA, (c) GO–PVA thin films, and (d) GO–PVA thin film in contact with carbaryl.

Based on the results obtained in Figure 8a,b, the RMS roughness for GO and PVA thin films were 6.7 nm and 7.9 nm, respectively. The 2D view of the AFM image of the GO thin film was relatively rough with the 3D view showing a lot of sharp peaks as compared to PVA thin film which displays a smoother appearance. The magnitude of immobilization of GO and PVA thin film increased in RMS roughness which was 8.5 nm as shown in Figure 8c. The presence of small white rod particles in the 2D image in Figure 8c was attributed to the GO immobilization of PVA. Subsequently, the RMS values of GO–PVA thin films were obtained at 9.7 nm when in contact with carbaryl, and the appearance displayed a

homogenous lattice and grid surface as shown in Figure 8d. The significant increase in RMS roughness of GO-PVA thin film after being in contact with carbaryl proved to be attributed to the interaction of GO-PVA with carbaryl.

3.4. Potential Sensing of Pesticide

In this study, an optical sensor based on SPR spectroscopy with Kretschmann configuration was performed. Firstly, the SPR angle for deionized water was determined at 53.5624° . The angle obtained was used as a reference to compare with the SPR angle for the various concentration of carbaryl solution ranging from 0.02 to 0.06 ppb. As shown in Figure 10, the SPR curves of carbaryl solution shifted from 0.02 to 0.06 ppb when compared to the SPR curve of deionized water. The SPR angle for 0.02, 0.04, and 0.06 ppb of carbaryl solution were 54.3988° , 54.6750° , and 54.9501° , respectively. Overall, the SPR shifted to the right as the concentration of carbaryl solution increased. Therefore, this experimental data indicates that gold-GO-PVA thin film has high sensitivity in the detection of carbaryl pesticides.

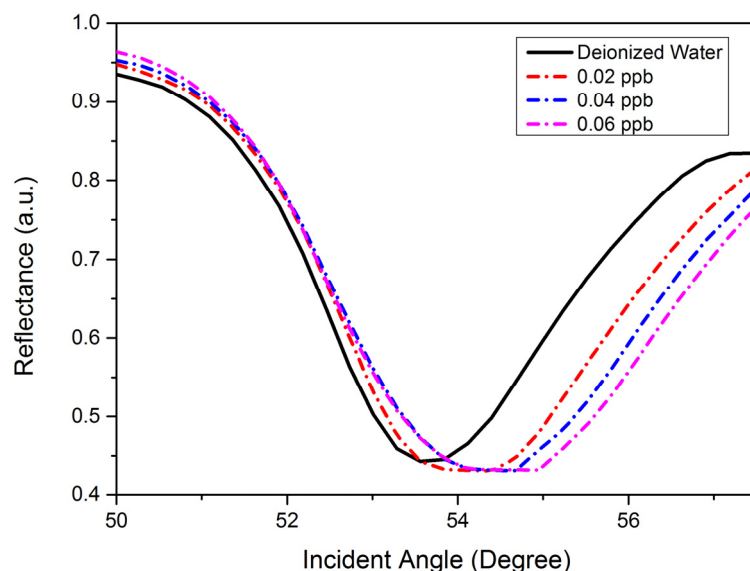


Figure 10. SPR reflectance curve for GO-PVA thin film in contact with various concentrations of carbaryl (0.02 ppb to 0.06 ppb).

4. Discussion

In the FTIR spectrum of GO-PVA thin film, the main functional group in GO and PVA elements such as C=O stretching, C=C stretching, $-\text{CH}_2$ stretching, C-O stretching, and O-H stretching were obtained, which indicated the interaction for both elements. To further reinforce this point, the formation of hydrogen bonding in the GO-PVA thin film will be emphasized. Basically, O-H stretching bands are sensitive to hydrogen bonds [157,158]. Therefore, the results of this study can conclude that the presence of hydrogen bond interaction with oxygen-containing GO and hydroxyl groups on the PVA chain is detrimental to the hydrogen bond between the PVA chains. It can be seen in Figure 3, the peak for O-H stretching shifts from 3771.67 cm^{-1} in pure PVA to lower wavenumbers of 3741.18 cm^{-1} , showing a decrease in hydrogen bonding among the hydroxyl groups in PVA chains.

In the following study, the UV-Vis spectroscopy result showed a high absorbance spectrum on the GO-PVA thin film in the range of 260 to 300 nm. It may be due to the homogeneous dispersion of GO in PVA, which allows for optimal UV light absorption. It could possibly be attributed to UV light scattered from the interface formed by hydrogen bonding between the GO and PVA on the gold thin film [159]. When GO was added to PVA, the band gap was reduced compared to the GO band gap. This could be related to the integration of GO's new energy levels that form between the conduction and valance

bands [160,161]. It also could interrupt the packing of polymer chains by GO resulting in a decrement of the crystallinity of the nanocomposites-polymer [162].

In order to visualize the GO, PVA, and GO–PVA thin films before and after contact with carbaryl, the AFM has been employed. Clearly, the thickness of immobilization GO and PVA thin film increased in RMS roughness which is 8.5 nm compared to a single element. This is attributed to the association of those two materials via hydrogen bonds formed between the oxygen-containing groups in GO and the hydroxyl groups in PVA [163]. This finding also shows that GO is well incorporated and dispersed in the PVA matrix and that it increases crystallinity by the increases the thickness. When the carbaryl was introduced to GO–PVA thin film, the RMS roughness was significantly increased to 9.7 nm. The combination of GO with PVA improved carbaryl adsorption, which increased the shift of resonance angle for this carbaryl solution. Hence, this result indicates that GO immobilized PVA can be used as a sensing element in the detection of carbaryl.

A better insight into the performance of the composite material to detect the carbaryl was accomplished by the SPR spectroscopy method. In this platform, the change in the resonance angle was observed for deionized water and various concentrations of carbaryl ranged from 0.02 ppb to 0.06 ppb. It can be seen that the SPR reflectance curve shifted to the right which indicated that the resonance angle increased with the increase of concentration carbaryl. This result is also attributable to analyte-ligand interaction, which is caused by changes in the refractive index and thickness of the GO–PVA sensing layer [164]. This is aligned with the AFM result, which shows that the presence of carbaryl alters the thickness of the sensing layer. Additionally, this study indicates that the sensitivity obtained is $13.78^\circ/\text{ppb}$. As a result, it is confirmed that GO–PVA thin film has a considerable positive correlation with carbaryl-based SPR optical sensor at a low concentration of 0.02 ppb.

The possible research directions for future work in this study may be considered in the selectivity of the composite material in the detection of carbaryl. This work also indicates that future work may be interested in carbaryl detection by using nanocomposites immobilization with a polymers-based SPR method without using any antibodies or enzymes in the fabrication of materials.

5. Comparison GO–PVA with Other Materials-Based Optical Methods to Detect Carbaryl

Thus far, most detection of carbaryl used antibodies and enzymes as the recognition element. There is no doubt that antibodies and enzymes have many advantages in various applications, especially in the field of biosensors [165,166]. However, they also have some drawbacks such as being expensive, complicated to prepare, requiring desirable storage properties, instability, and poor reproducibility [167–169]. To address the mentioned issues, this work for the first time proposes the use of GO–PVA thin film as a sensing element that is inexpensive, requires simple preparation, is easy to operate, more stable, repeatable, and, most importantly, has a high sensitivity. The comparison of the performance of this composite material compared to the previous study that used various materials to detect carbaryl based on the optical method is given in the table below. Based on Table 1, it can be concluded that the development of of a carbaryl pesticide detection-based optical method has attracted extensive research interest with the use of various materials including molecular imprinted polymer, metal oxide, and quantum dots. It also can be seen that the GO–PVA sensing layer has the lowest limit of detection compared to the others. Therefore, this work indicates that polymer nanocomposites prove to be a good candidate for carbaryl detection at a low level.

Table 1. Comparison of the lowest detection carbaryl with various material-based optical sensors.

Materials	Limit of Detection	References
4-acetamidobenzenesulfonyl azide-AuNPs	50.00 ppb	[170]
acetylcholinesterase	20.00 ppb	[171]
3,5-di(2',5'-dicarboxylphenyl)pyridine	6.70 ppb	[172]
idophenyl acetate-acetylcholinesterase	2.01 ppb	[173]
silver reduced-graphene oxide	1.50 ppb	[174]
monoclonal antibody	1.41 ppb	[175]
monoclonal antibody	1.38 ppb	[176]
flavourzyme-stabilized gold nanoclusters	0.47 ppb	[177]
graphene quantum dots	0.36 ppb	[178]
carbon quantum dots-AuNPs-acetylcholinesterase	0.20 ppb	[179]
cadmium tellurite quantum dots	0.12 ppb	[180]
monoclonal antibody	0.05 ppb	[181]
cadmium selenide/zinc sulfide quantum dots	0.03 ppb	[182]
graphene oxide-polyvinyl alcohol	0.02 ppb	This study

6. Conclusions

According to the results stated above, the characterization properties of the graphene oxide–polyvinyl alcohol (GO–PVA) thin film were successfully synthesized and investigated. These research results also represent the first milestone in sensing performance for GO–PVA thin film in the detection carbaryl-based-SPR method. From the investigation of structural properties by FTIR, the result confirmed that the surface interaction between GO and PVA thin film as the main functional group was obtained with the composite material. Then the UV-Vis was employed to investigate the optical properties. The UV-Vis result obtained high absorption and a lower band gap value in GO–PVA thin film compared to the GO single element. Next, the surface morphology was analyzed by AFM, which validates the interaction of the GO–PVA thin film and carbaryl based on the increment in the thickness. Meanwhile, the as-prepared GO–PVA thin film exhibited a good sensing performance-based SPR method when the reflected curve shifted to the right with the increased concentration of carbaryl. This result indicates the high sensitivity in the detection of carbaryl by the composite material. The high sensitivity of the SPR sensor makes this GO–PVA an appealing recognition element for carbaryl detection while also opening up a new path for pesticide sensor applications based on nanomaterials and polymers.

Author Contributions: Conceptualization, N.I.M.F.; methodology, N.A.S.O.; software, W.M.E.M.M.D.; validation, Y.W.F.; formal analysis, F.B.K.E.; investigation, N.I.M.F.; resources, M.A.K.; writing—original draft preparation, N.I.M.F.; writing—review and editing, Y.W.F.; visualization, W.M.E.M.M.D. and N.S.M.R.; supervision, Y.W.F. and J.A.; funding acquisition, Y.W.F. All authors have read and agreed to the published version of the manuscript.

Funding: This research was funded by Ministry of Education Malaysia through the Fundamental Research Grant Scheme (FRGS) (FRGS/1/2019/STG02/UPM/02/1) and the APC was funded by Universiti Putra Malaysia.

Institutional Review Board Statement: Not applicable.

Informed Consent Statement: Not applicable.

Data Availability Statement: Data sharing is not applicable in this article.

Acknowledgments: The authors are grateful to the Institute of Nanoscience and Nanotechnology, Department of Physics and Department of Chemistry, Faculty of Science, Universiti Putra Malaysia for providing all the facilities.

Conflicts of Interest: The authors declare no conflict of interest.

References

1. Lieberzeit, P.A.; Dickert, F.L. Sensor technology and its application in environmental analysis. *Anal. Bioanal. Chem.* **2007**, *387*, 237–247. [[CrossRef](#)] [[PubMed](#)]
2. Kerschen, G.; De Boe, P.; Golinval, J.; Worden, K. Sensor validation using principal component analysis. *Smart Mater. Struct.* **2005**, *14*, 36–42. [[CrossRef](#)]
3. Abdollahzadeh, S.; Navimipour, N.J. Deployment strategies in the wireless sensor network: A comprehensive review. *Comput. Commun.* **2016**, *91–92*, 1–16.
4. Zakaria, R.; Zainuddin, N.M.; Fahri, M.A.S.A.; Thirunavakkarasu, P.M.; Patel, S.K.; Harun, S.W. High sensitivity refractive index sensor in long-range surface plasmon resonance based on side polished optical fiber. *Opt. Fiber Technol.* **2021**, *61*, 102449.
5. Souto, D.E.; Volpe, J.; Goncalves, C.d.C.; Ramos, C.H.I.; Kubota, L.T. A brief review on the strategy of developing SPR-based biosensors for application to the diagnosis of neglected tropical diseases. *Talanta* **2019**, *205*, 120122. [[CrossRef](#)] [[PubMed](#)]
6. Verma, R.K.; Suwalka, P.; Yadav, J. Detection of adulteration in diesel and petrol by kerosene using SPR based fiber optic technique. *Opt. Fiber Technol.* **2018**, *43*, 95–100. [[CrossRef](#)]
7. Takemura, K. Surface Plasmon Resonance (SPR)- and localized spr (lspr)-based virus sensing systems: Optical vibration of nano- and micro-metallic materials for the development of next-generation virus detection technology. *Biosensors* **2021**, *11*, 250. [[CrossRef](#)]
8. Semwal, V.; Gupta, B.D. Highly selective SPR based fiber optic sensor for the detection of hydrogen peroxide. *Sens. Actuators B Chem.* **2020**, *329*, 129062. [[CrossRef](#)]
9. Xie, S.; Wang, X.; Shang, H. Security analysis on wireless sensor network in the data center for energy internet of things. *Int. J. Saf. Secur. Eng.* **2020**, *10*, 397–402. [[CrossRef](#)]
10. Wang, S.; Ding, L.; Wang, Y.; Gong, X. Multifunctional triboelectric nanogenerator towards impact energy harvesting and safeguards. *Nano Energy* **2019**, *59*, 434–442. [[CrossRef](#)]
11. Rhazouani, A.; Gamrani, H.; El Achaby, M.; Aziz, K.; Gebrati, L.; Uddin, S.; Aziz, F. Synthesis and toxicity of graphene oxide nanoparticles: A literature review of in vitro and in vivo studies. *BioMed Res. Int.* **2021**, *2021*, 5518999. [[CrossRef](#)] [[PubMed](#)]
12. Aliyev, E.; Filiz, V.; Khan, M.M.; Lee, Y.J.; Abetz, C.; Abetz, V. Structural characterization of graphene oxide: Surface functional groups and fractionated oxidative debris. *Nanomaterials* **2019**, *9*, 1180. [[CrossRef](#)] [[PubMed](#)]
13. Shahriary, L.; Athawale, A.A. Graphene oxide synthesized by using modified hummers approach. *Int. J. Renew. Energy Environ. Eng.* **2014**, *2*, 58–63.
14. Claramunt, S.; Varea, A.; Lopez-Diaz, D.; Velazquez, M.M.; Cornet, A.; Cirera, A. The importance of interbands on the interpretation of the raman spectrum of graphene oxide. *J. Phys. Chem.* **2015**, *119*, 10123–10129. [[CrossRef](#)]
15. Mattevi, C.; Eda, G.; Agnoli, S.; Miller, S.; Mkhoyan, K.A.; Celik, O.; Mastrogiovanni, D.; Granozzi, G.; Garfunkel, E.; Chhowalla, M. Evolution of electrical, chemical, and structural properties of transparent and conducting chemically derived graphene thin films. *Adv. Funct. Mater.* **2009**, *19*, 2577–2583. [[CrossRef](#)]
16. Perrozzi, F.; Prezioso, S.; Ottaviano, L. Graphene oxide: From fundamentals to applications. *J. Phys. Condens. Matter* **2015**, *27*, 13002. [[CrossRef](#)]
17. Ling, S. Structure and synthesis of graphene oxide. *Chin. J. Chem. Eng.* **2019**, *27*, 2251–2260.
18. Huang, X.; Liu, L.; Zhou, S.; Zhao, J. Physical properties and device applications of graphene oxide. *Front. Phys.* **2019**, *15*, 33301. [[CrossRef](#)]
19. Sun, M.; Li, J. Graphene oxide membranes: Functional structures, preparation and environmental applications. *Nano Today* **2018**, *20*, 121–137. [[CrossRef](#)]
20. Zhao, J.; Dehbari, N.; Han, W.; Huang, L.; Tang, Y. Electrospun multi-scale hybrid nano fiber/net with enhanced water swelling ability in rubber composites. *Mater. Des.* **2015**, *86*, 14–21. [[CrossRef](#)]
21. Chen, X.; Qiu, M.; Ding, H.; Fu, K.; Fan, Y. Reduced graphene oxide nanofiltration membrane intercalated by well-dispersed carbon nanotubes for drinking water purification. *Nanoscale* **2016**, *8*, 5696–5705. [[CrossRef](#)] [[PubMed](#)]
22. Yang, X.; Tu, Y.; Li, L.; Shang, S.; Tao, X. Well-dispersed chitosan/graphene oxide nanocomposites. *Appl. Mater. Interfaces* **2010**, *2*, 1707–1713. [[CrossRef](#)] [[PubMed](#)]
23. Shen, J.; Hu, Y.; Li, C.; Qin, C.; Ye, M. Synthesis of amphiphilic graphene nanoplatelets. *Communications* **2009**, *4*, 82–85. [[CrossRef](#)] [[PubMed](#)]
24. Kim, F.; Cote, L.J.; Huang, J. Graphene Oxide: Surface Activity and Two-Dimensional assembly. *Adv. Mater.* **2010**, *22*, 1954–1958. [[CrossRef](#)]
25. Huang, T.; Zeng, X.; Yao, Y.; Sun, R.; Meng, F.; Xu, J.; Wong, C. Boron nitride@graphene oxide hybrids for epoxy composites with enhanced thermal conductivity. *RSC Adv.* **2016**, *6*, 35847–35854. [[CrossRef](#)]
26. Yeh, C.; Raidongia, K.; Shao, J.; Yang, Q.; Huang, J. On the origin of the stability of graphene oxide membranes in water. *Nat. Chem.* **2015**, *7*, 166–170. [[CrossRef](#)] [[PubMed](#)]
27. Mohan, V.B.; Lau, K.; Hui, D.; Bhattacharyya, D. Graphene-based materials and their composites: A review on production, applications and product limitations. *Compos. Part B* **2018**, *142*, 200–220. [[CrossRef](#)]
28. Kim, J.; Cote, L.J.; Kim, F.; Yuan, W.; Shull, K.R.; Huang, J. Graphene oxide sheets at interfaces. *JACS Artic.* **2010**, *132*, 8180–8186. [[CrossRef](#)]

29. Kim, J.; Cote, L.J.; Huang, J. Two dimensional soft material: New faces of graphene oxide. *Acc. Chem. Res.* **2012**, *45*, 1356–1364. [[CrossRef](#)]
30. Achari, A.; Datta, K.K.R.; De, M.; Dravid, V.P.; Eswaramoorthy, M. Amphiphilic Aminoclay-rGO hybrids: A simple strategy to disperse a high concentration of rGO in water. *Nanoscale* **2010**, *5*, 5316–5320. [[CrossRef](#)]
31. Dong, X.; Huang, W.; Chen, P. In situ synthesis of reduced graphene oxide and gold nanocomposites for nanoelectronics and biosensing. *Nanoscale Res. Lett.* **2011**, *6*, 60. [[CrossRef](#)] [[PubMed](#)]
32. Ho, K.; Huang, C.; Liao, J.; Zhang, W.; Li, L.; Lai, C.; Su, C. Fluorinated graphene as high performance dielectric materials and the applications for graphene nanoelectronics. *Sci. Rep.* **2014**, *4*, 5893. [[CrossRef](#)] [[PubMed](#)]
33. Wang, Y.; Chen, Z.; Huang, J.; Li, G.; Cao, J.; Zhang, B.; Chen, X.; Zhang, H.; Jia, L. Preparation and catalytic behavior of reduced graphene oxide supported cobalt oxide hybrid nanocatalysts for CO oxidation. *Trans. Nonferrous Met. Soc. China* **2018**, *28*, 2265–2273. [[CrossRef](#)]
34. Yang, M.; Zhou, M.; Zhang, A.; Zhang, C. Graphene oxide: An ideal support for gold nanocatalysts. *J. Phys. Chem.* **2012**, *116*, 22336–22340. [[CrossRef](#)]
35. Gupta, V.K.; Atar, N.; Yola, M.L.; Üstündağ, Z.; Uzun, L. A novel magnetic Fe@Au core-shell nanoparticles anchored graphene oxide recyclable nanocatalyst for the reduction of nitrophenol compounds. *Water Res.* **2013**, *48*, 210–217. [[CrossRef](#)] [[PubMed](#)]
36. Wang, H.; Li, S.; Si, Y.; Zhang, N.; Sun, Z.; Wu, H.; Lin, Y. Platinum nanocatalysts loaded on graphene oxide- dispersed carbon nanotubes with greatly enhanced peroxidase-like catalysis and electrocatalysis. *Nanoscale* **2014**, *6*, 17–19. [[CrossRef](#)] [[PubMed](#)]
37. Hsieh, C.; Chen, W.; Tzou, D.; Roy, A.K.; Hsiao, H. Atomic layer deposition of Pt nanocatalysts on graphene oxide nanosheets for electro-oxidation of formic acid. *Int. J. Hydrogen Energy* **2012**, *37*, 17837–17843. [[CrossRef](#)]
38. Maleki, A.; Paydar, R. Graphene oxide–chitosan bionanocomposite: A highly efficient nanocatalyst for the one-pot three-component synthesis of trisubstituted imidazoles under solvent-free conditions. *RSC Adv.* **2015**, *5*, 33177–33184. [[CrossRef](#)]
39. Lin, B.; Chen, H.; Liang, D.; Lin, W.; Qi, X.; Liu, H.; Deng, X. Acidic pH and High-H₂O₂ dual tumor microenvironment-responsive nanocatalytic graphene oxide for cancer selective therapy and recognition. *ACS Appl. Mater. Interfaces* **2019**, *11*, 11157–11166. [[CrossRef](#)]
40. Smith, A.T.; Marie, A.; Zeng, S.; Liu, B.; Sun, L. Nano materials science synthesis, properties, and applications of graphene oxide/reduced graphene oxide and their nanocomposites. *Nano Mater. Sci.* **2019**, *1*, 31–47. [[CrossRef](#)]
41. Zhu, Y.; Murali, S.; Cai, W.; Li, X.; Suk, J.W.; Potts, J.R.; Ruoff, R.S. Graphene and graphene oxide: Synthesis, properties, and applications. *Adv. Mater.* **2010**, *22*, 3906–3924. [[CrossRef](#)] [[PubMed](#)]
42. Chen, D.; Feng, H.; Li, J. Graphene oxide: Preparation, functionalization, and electrochemical applications. *Chem. Rev.* **2004**, *112*, 6027–6053. [[CrossRef](#)] [[PubMed](#)]
43. Dong, X.; Xing, G.; Chan-park, M.B.; Shi, W.; Xiao, N.; Wang, J.; Yan, Q.; Sum, T.C.; Huang, W.; Chen, P. The formation of a carbon nanotube–graphene oxide core–shell structure and its possible applications. *Carbon* **2011**, *49*, 5071–5078. [[CrossRef](#)]
44. Zuo, X.; He, S.; Li, D.; Peng, C.; Huang, Q.; Song, S.; Fan, C. Graphene oxide-facilitated electron transfer of metalloproteins at electrode surfaces. *Langmuir* **2010**, *26*, 1936–1939. [[CrossRef](#)]
45. Chen, Y.; Chen, L.; Bai, H.; Li, L. Graphene oxide–chitosan composite hydrogels as broad-spectrum adsorbents for water purification. *J. Mater. Chem. A* **2013**, *1*, 1992–2001. [[CrossRef](#)]
46. Dinda, D.; Gupta, A.; Saha, S.K. Removal of toxic Cr(VI) by UV-active functionalized graphene oxide for water purification. *J. Mater. C* **2013**, *1*, 11221–11228. [[CrossRef](#)]
47. Yin, J.; Zhu, G.; Deng, B. Graphene oxide (GO) enhanced polyamide (PA) thin-film nanocomposite (TFN) membrane for water purification. *Desalination* **2016**, *379*, 93–101. [[CrossRef](#)]
48. Xu, Q.; Xu, H.; Chen, J.; Lv, Y.; Dong, C.; Sreeprasad, T.S. Graphene and graphene oxide: Advanced membranes for gas separation and water purification. *Inorg. Chem. Front.* **2015**, *2*, 417–424. [[CrossRef](#)]
49. Ain, Q.; Farooq, M.U.; Jalees, M.I. Application of magnetic graphene oxide for water purification: Heavy metals removal and disinfection. *J. Water Process Eng.* **2020**, *33*, 101044. [[CrossRef](#)]
50. Xu, C.; Cui, A.; Xu, Y.; Fu, X. Graphene oxide–TiO₂ composite filtration membranes and their potential application for water purification. *Carbon* **2013**, *62*, 465–471. [[CrossRef](#)]
51. Fathizadeh, M.; Xu, W.L.; Zhou, F.; Yoon, Y.; Yu, M. Graphene Oxide: A novel 2-dimensional material in membrane separation for water purification. *Adv. Mater. Interfaces* **2017**, *4*, 1600918. [[CrossRef](#)]
52. Sun, X.; Qin, J.; Xia, P.; Guo, B.; Yang, C.; Song, C.; Wang, S.-G. Graphene oxide-silver nanoparticle membrane for biofouling control and water purification. *Chem. Eng. J.* **2015**, *281*, 53–59. [[CrossRef](#)]
53. Al-gamal, A.Q.; Falath, W.S.; Saleh, T.A. Enhanced efficiency of polyamidemembranes by incorporating TiO₂-Graphene oxide for water purification. *J. Mol. Liq.* **2021**, *323*, 114922. [[CrossRef](#)]
54. Chung, C.; Kim, Y.; Shin, D.; Ryoo, S.; Hong, B.H.; Min, D. Biomedical applications of graphene and graphene oxide. *Acc. Chem. Res.* **2013**, *46*, 2211–2224. [[CrossRef](#)] [[PubMed](#)]
55. Liu, J.; Cui, L.; Losic, D. Graphene and graphene oxide as new nano-carriers for drug delivery applications. *Acta Biomater.* **2013**, *9*, 9243–9257. [[CrossRef](#)] [[PubMed](#)]
56. Ye, Y.; Mao, X.; Xu, J.; Kong, J.; Hu, X. Functional graphene oxide nanocarriers for drug delivery. *Int. J. Polym. Sci.* **2019**, *2019*, 8453493. [[CrossRef](#)]

57. Sun, X.; Liu, Z.; Welsher, K.; Robinson, J.T.; Goodwin, A.; Zaric, S.; Dai, H. Nano-graphene oxide for cellular imaging and drug delivery. *Nano Res.* **2008**, *1*, 203–212. [[CrossRef](#)]
58. Weaver, C.L.; Larosa, J.M.; Luo, X.; Cui, X.T. Electrically controlled drug delivery from graphene oxide nanocomposite films. *ACS Nano* **2014**, *8*, 1834–1843. [[CrossRef](#)]
59. Cheng, S.-J.; Chiu, H.-Y.; Kumar, P.V.; Hsieh, K.Y.; Yang, J.-W.; Lin, Y.-R.; Shen, Y.-C.; Chen, G.-Y. Simultaneous drug delivery and cellular imaging using graphene oxide. *Biomater. Sci.* **2018**, *6*, 813–819. [[CrossRef](#)]
60. Makharza, S.; Cirillo, G.; Bachmatiuk, A.; Ibrahim, I.; Ioannides, N.; Trzebicka, B.; Hampel, S.; Rummeli, M.H. Graphene oxide-based drug delivery vehicles: Functionalization, characterization, and cytotoxicity evaluation. *J. Nanopart. Res.* **2013**, *15*, 2099. [[CrossRef](#)]
61. Yang, Y.; Zhang, Y.; Chen, Y.; Zhao, D.; Chen, J.; Liu, Y. Construction of a graphene oxide based noncovalent multiple nanosupramolecular assembly as a scaffold for drug delivery. *Chem. A Eur. J.* **2012**, *18*, 4208–4215. [[CrossRef](#)] [[PubMed](#)]
62. Daniyal, W.M.E.M.M.; Fen, Y.W.; Abdullah, J.; Sadrolhosseini, A.R.; Saleviter, S.; Omar, N.A.S. Label-free optical spectroscopy for characterizing binding properties of highly sensitive nanocrystalline cellulose-graphene oxide based nanocomposite towards nickel ion. *Spectrochim. Acta Part A Mol. Biomol. Spectrosc.* **2018**, *212*, 25–31. [[CrossRef](#)] [[PubMed](#)]
63. Zainudin, A.A.; Fen, Y.W.; Yusof, N.A.; Omar, N.A.S. Structural, optical and sensing properties of ionophore doped graphene based bionanocomposite thin film. *Optik* **2017**, *144*, 308–315. [[CrossRef](#)]
64. Hashim, H.S.; Fen, Y.W.; Omar, N.A.S.; Abdullah, J.; Daniyal, W.M.E.M.M.; Saleviter, S. Detection of phenol by incorporation of gold modified-enzyme based graphene oxide thin film with surface plasmon resonance technique. *Opt. Express* **2020**, *28*, 9738–9752. [[CrossRef](#)] [[PubMed](#)]
65. Roshidi, M.D.A.; Fen, Y.W.; Omar, N.A.S.O.; Saleviter, S.; Daniyal, W.M.E.M.M. Optical studies of graphene oxide/poly(amidoamine) dendrimer composite thin film and its potential for sensing Hg²⁺ using surface plasmon resonance spectroscopy. *Sens. Mater.* **2019**, *31*, 1147–1156.
66. Daniyal, W.M.E.M.M.; Fen, Y.W.; Abdullah, J.; Saleviter, S.; Omar, N.A.S. Preparation and characterization of hexadecyltrimethylammonium bromide modified nanocrystalline cellulose/graphene oxide composite thin film and its potential in sensing copper ion using surface plasmon resonance technique. *Opt.-Int. J. Light Electron. Opt.* **2018**, *173*, 71–77. [[CrossRef](#)]
67. Omar, N.A.S.; Fen, Y.W.; Saleviter, S.; Daniyal, W.M.E.M.M.; Anas, N.A.A.; Ramdzan, N.S.M.; Roshidi, M.D.A. Development of a graphene-based surface plasmon resonance optical sensor chip for potential biomedical application. *Materials* **2019**, *12*, 1928. [[CrossRef](#)]
68. Anas, N.A.A.; Fen, Y.W.; Omar, N.A.S. Development of graphene quantum dots-based optical sensor for toxic metal ion detection. *Sensors* **2019**, *19*, 3850. [[CrossRef](#)]
69. Saleviter, S.; Fen, Y.W.; Omar, N.A.S.; Zainudin, A.A.; Daniyal, W.M.E.M.M. Optical and structural characterization of immobilized 4-(2-pyridylazo)resorcinol in chitosan-graphene oxide composite thin film and its potential for Co²⁺ sensing using surface plasmon resonance technique. *Results Phys.* **2018**, *11*, 118–122. [[CrossRef](#)]
70. Anas, N.A.A.; Fen, Y.W.; Omar, N.A.S.; Ramdzan, N.S.M.; Daniyal, W.M.E.M.M.; Saleviter, S.; Zainuddin, A.A. Optical properties of chitosan/hydroxyl-functionalized graphene quantum dots thin film for potential optical detection of ferric (III) ion. *Opt. Laser Technol.* **2019**, *120*, 105724. [[CrossRef](#)]
71. Saleviter, S.; Fen, Y.W.; Omar, N.A.S.; Daniyal, W.M.E.M.M.; Abdullah, J.; Zaid, M.H.M. Structural and optical studies of cadmium sulfide quantum dot- graphene oxide-chitosan nanocomposite thin film as a novel spr spectroscopy active layer. *J. Nanomater.* **2018**, *2018*, 4324072. [[CrossRef](#)]
72. Anas, N.A.A.; Fen, Y.W.; Yusof, N.A.; Omar, N.A.S.; Ramdzan, N.S.M.; Daniyal, W.M.E.M.M. Investigating the properties of cetyltrimethylammonium bromide/hydroxylated graphene quantum dots thin film for potential optical detection of heavy metal ions. *Materials* **2020**, *13*, 2591.
73. Hashim, H.S.; Fen, Y.W.; Omar, N.A.S.; Fauzi, N.I.M.; Daniyal, W.M.E.M.M. Recent advances of priority phenolic compounds detection using phenol oxidases-based electrochemical and optical sensors. *Measurement* **2021**, *184*, 109855. [[CrossRef](#)]
74. Zainudin, A.A.; Fen, Y.W.; Yusof, N.A.; Al-Rekabi, S.H.; Mahdi, M.A.; Omar, N.A.S. Incorporation of surface plasmon resonance with novel valinomycin doped chitosan-graphene oxide thin film for sensing potassium ion. *Spectrochim. Acta-Part A Mol. Biomol. Spectrosc.* **2018**, *191*, 111–115. [[CrossRef](#)]
75. Li, D.; Wang, T.; Li, Z.; Xu, X.; Wang, C.; Duan, Y. Application of graphene-based materials for detection of nitrate and nitrite in water—A Review. *Sensors* **2019**, *20*, 54. [[CrossRef](#)]
76. Joshi, D.J.; Janardhan, K.R.; Malek, N.I.; Hussain, C.M.; Kumar, K.S. Surface modifications and analytical applications of graphene oxide: A review. *Trends Anal. Chem.* **2021**, *144*, 116448. [[CrossRef](#)]
77. Hegab, H.M.; Zou, L. Graphene oxide-assisted membranes: Fabrication and potential applications in desalination and water purification. *J. Memb. Sci.* **2015**, *484*, 95–106. [[CrossRef](#)]
78. Harsanyi, G. Polymer films in sensor applications: A review of present uses and future possibilities. *Sens. Rev.* **2000**, *20*, 98–105. [[CrossRef](#)]
79. Arul, K.T.; Manikandan, E.; Ladchumananandasivam, R.; Maaza, M. Novel PVA polymer based nanostructure with ferrities co-doped with nickel and cobalt ions for Magneto-Sensor application. *Polym. Int.* **2016**, *65*, 1482–1485. [[CrossRef](#)]
80. Ansari, S. Combination of molecularly imprinted polymers and carbon nanomaterials as a versatile biosensing tool in sample analysis: Recent applications and challenges. *Trends Anal. Chem.* **2017**, *93*, 134–151. [[CrossRef](#)]

81. Feig, V.R.; Tran, H.; Bao, Z. Biodegradable polymeric materials in degradable electronic devices. *ACS Cent. Sci.* **2018**, *4*, 337–348. [[CrossRef](#)] [[PubMed](#)]
82. Li, S.; Cao, S.; Whitcombe, M.J.; Piletsky, S.A. Size matters: Challenges in imprinting macromolecules. *Prog. Polym. Sci.* **2014**, *39*, 145–163. [[CrossRef](#)]
83. Mallakpour, S.; Dinari, M. Progress in synthetic polymers based on natural amino progress in synthetic polymers based on natural amino acids. *J. Macromol. Sci. Part A Pure Appl. Chem.* **2011**, *48*, 37–41. [[CrossRef](#)]
84. Hu, K.; Kulkarni, D.D.; Choi, I.; Tsukruk, V.V. Graphene–polymer nanocomposites for structural and functional applications. *Prog. Polym. Sci.* **2014**, *39*, 1934–1972. [[CrossRef](#)]
85. Cai, D.; Song, M. Recent advance in functionalized graphene/polymer nanocomposites. *J. Mater. Chem.* **2010**, *20*, 7906. [[CrossRef](#)]
86. Potts, J.R.; Dreyer, D.R.; Bielawski, C.W.; Ruoff, R.S. Graphene-based polymer nanocomposites. *Polymer* **2011**, *52*, 5–25. [[CrossRef](#)]
87. Verdejo, R.; Bernal, M.M.; Romasanta, L.J.; Lopez-manchado, M.A. Graphene filled polymer nanocomposites. *J. Mater. Chem.* **2011**, *21*, 3301–3310. [[CrossRef](#)]
88. Zhang, M.; Li, Y.; Su, Z.; Wei, G. Recent advances in the synthesis and applications of graphene-polymer nanocomposites. *Polym. Chem.* **2015**, *6*, 6107–6124. [[CrossRef](#)]
89. Cui, Y.; Kundalwal, S.I.; Kumar, S. Gas barrier performance of graphene/polymer nanocomposites. *Carbon* **2016**, *98*, 313–333. [[CrossRef](#)]
90. Vickery, J.L.; Patil, A.J.; Mann, S. Fabrication of graphene—Polymer nanocomposites with higher-order three-dimensional architectures. *Adv. Mater.* **2009**, *21*, 2180–2184. [[CrossRef](#)]
91. Ramanathan, T.; Abdala, A.A.; Stankovich, S.; Dikin, D.A.; Herrera-Alonso, M.; Piner, R.D.; Adamson, D.H.; Schniepp, H.C.; Chen, X.; Ruoff, R.S.; et al. Functionalized graphene sheets for polymer nanocomposites. *Letters* **2008**, *3*, 327–331. [[CrossRef](#)] [[PubMed](#)]
92. Liu, J.; Ye, Y.; Xue, Y.; Xie, X.; Mai, Y. Recent Advances in covalent functionalization of carbon nanomaterials with polymers: Strategies and perspectives. *J. Polym. Sci. Part A Polym. Chem.* **2016**, *55*, 622–631. [[CrossRef](#)]
93. Yoo, B.M.; Shin, H.J.; Yoon, H.W.; Park, H.B. Graphene and graphene oxide and their uses in barrier polymers. *J. Polym. Sci. Part A Polym. Chem.* **2013**, *131*, 1–23. [[CrossRef](#)]
94. Li, D.; Huang, J.; Kaner, R.B. Polyaniline nanofibers: A unique polymer nanostructure for versatile applications. *Acc. Chem. Res.* **2009**, *42*, 135–145. [[CrossRef](#)] [[PubMed](#)]
95. Aslam, M.; Kalyar, M.A.; Raza, Z.A. Polyvinyl alcohol: A review of research status and use of polyvinyl alcohol based nanocomposites. *Polym. Eng. Sci.* **2018**, *58*, 2119–2132. [[CrossRef](#)]
96. Gaaz, T.S.; Sulong, A.B.; Akhtar, M.N.; Kadhum, A.A.H.; Mohamad, A.B.; Al-Amiery, A.A. Properties and applications of polyvinyl alcohol, halloysite nanotubes and their nanocomposites. *Molecules* **2015**, *20*, 22833–22847. [[CrossRef](#)]
97. Chang, I.; Kim, C.; Nam, B. The influence of poly-vinyl-alcohol (PVA) characteristics on the physical stability of encapsulated immobilization media for advanced wastewater treatment. *Process Biochem.* **2005**, *40*, 3050–3054. [[CrossRef](#)]
98. Aziz, S.B.; Hassan, A.Q.; Mohammed, S.J.; Karim, W.O.; Kadir, M.F.Z.; Tajuddin, H.A.; Chan, N.N.M.Y. Structural and optical characteristics of PVA: C-Dot Composites: Tuning the absorption of ultra violet (UV) region. *Nanomaterials* **2019**, *9*, 216. [[CrossRef](#)]
99. Liu, F.; Xu, K.; Ding, W.; Qiao, Y.; Wang, L. Microstructural characteristics and their impact on mechanical properties of steel-PVA fiber reinforced concrete. *Cem. Concr. Compos.* **2021**, *123*, 104196. [[CrossRef](#)]
100. Rudra, R.; Kumar, V.; Kundu, P.P. Acid catalysed cross-linking of poly vinyl alcohol (PVA) by glutaraldehyde: Effect of crosslink density on the characteristics of PVA membrane used in single chambered microbial fuel cell. *RSC Adv.* **2015**, *5*, 83436–83447. [[CrossRef](#)]
101. Hakalahti, M.; Salminen, A.; Seppälä, J.; Tammelin, T.; Hanninen, T. Effect of interfibrillar PVA bridging on water stability and mechanical properties of TEMPO/NaClO₂ oxidized cellulosic nanofibril films. *Carbohydr. Polym.* **2015**, *126*, 78–82. [[CrossRef](#)] [[PubMed](#)]
102. Kochkina, N.E.; Lukin, N.D. Structure and properties of biodegradable maize starch/chitosan composite films as affected by PVA additions. *Int. J. Biol. Macromol.* **2020**, *157*, 377–384. [[CrossRef](#)] [[PubMed](#)]
103. Shi, G.; Araby, S.; Gibson, C.T.; Meng, Q.; Zhu, S.; Ma, J. Graphene platelets and their polymer composites: Fabrication, structure, properties, and applications. *Adv. Funct. Mater.* **2018**, *28*, 1706705. [[CrossRef](#)]
104. Gudarzi, M.M.; Sharif, F. Enhancement of dispersion and bonding of graphene-polymer through wet transfer of functionalized graphene oxide. *Express Polym. Lett.* **2012**, *6*, 1017–1031. [[CrossRef](#)]
105. Gudarzi, M.M.; Moghadam, M.H.M.; Sharif, F. Spontaneous exfoliation of graphite oxide in polar aprotic solvents as the route to produce graphene oxide—Organic solvents liquid crystals. *Carbon* **2013**, *64*, 403–415. [[CrossRef](#)]
106. Khan, Z.U.; Kausar, A.; Ullah, H.; Badshah, A. A review of graphene oxide, graphene buckypaper, and polymer/graphene composites: Properties and fabrication techniques. *J. Plast. Film Sheeting* **2016**, *32*, 336–379. [[CrossRef](#)]
107. Bhawal, P.; Ganguly, S.; Chaki, T.K.; Das, N.C. Synthesis and characterization of graphene oxide filled ethylene methyl acrylate hybrid nanocomposites. *RSC Adv.* **2016**, *6*, 20781–20790. [[CrossRef](#)]
108. Badri, A.; Whittaker, M.R.; Zetterlund, P.B. Modification of graphene/graphene oxide with polymer brushes using controlled/living radical polymerization. *Polym. Chem.* **2012**, *50*, 2981–2992. [[CrossRef](#)]

109. Zhang, S.; Liu, P.; Zhao, X.; Xu, J. Preparation of poly (vinyl alcohol)-grafted graphene oxide/poly (vinyl alcohol) Nanocomposites via in-situ low-temperature emulsion polymerization and their thermal and mechanical characterization. *Appl. Surf. Sci.* **2016**, *396*, 1098–1107. [[CrossRef](#)]
110. Govindaraj, P.; Sokolova, A.; Salim, N.; Juodkazis, S.; Konstantin, F.; Fox, B.; Hameed, N. Distribution states of graphene in polymer nanocomposites: A review. *Compos. Part B* **2021**, *226*, 109353. [[CrossRef](#)]
111. Hurayra-Lizu, A.K.M.; Bari, W.M.D.; Gulshan, F.; Islam, R.M. GO based PVA nanocomposites: Tailoring of optical and structural properties of PVA with low percentage of GO nano fillers. *Heliyon* **2021**, *7*, e06983. [[CrossRef](#)] [[PubMed](#)]
112. Liang, J.; Huang, Y.; Zhang, L.; Wang, Y.; Ma, Y.; Guo, T.; Chen, Y. Molecular-level dispersion of graphene into poly(vinyl alcohol) and effective reinforcement of their nanocomposites. *Adv. Funct. Mater.* **2009**, *19*, 2297–2302. [[CrossRef](#)]
113. Al Sheheri, S.Z.; Al-amshany, Z.M.; Al Sulami, Q.A.; Tashkandi, N.Y.; Hussein, M.A.; El-shishtawy, R.M. The preparation of carbon nanofillers and their role on the performance of variable polymer nanocomposites. *Des. Monomers Polym.* **2019**, *22*, 8–53. [[CrossRef](#)]
114. Shi, Y.; Xiong, D.; Li, J.; Wang, N. In situ reduction of graphene oxide nanosheets in poly(vinyl alcohol) hydrogel by γ -ray irradiation and its influence on mechanical and tribological properties. *J. Phys. Chem.* **2016**, *120*, 19442–194543. [[CrossRef](#)]
115. Qi, Y.Y.; Tai, Z.X.; Sun, D.F.; Chen, J.T.; Ma, H.B.; Yan, X.B.; Liu, B.; Xue, Q.J. Fabrication and characterization of poly(vinyl alcohol)/graphene oxide nanofibrous biocomposite scaffolds. *J. Appl. Polym.* **2012**, *127*, 1885–1894. [[CrossRef](#)]
116. Sun, Y.; Lu, J.; Ai, C.; Wen, D. Nonvolatile memory devices based on poly(vinyl alcohol) + graphene oxide hybrid composites. *Phys. Chem. Chem. Phys.* **2016**, *18*, 11341–11347. [[CrossRef](#)]
117. Debnath, D.; Zhao, X.; Anas, M.; Kulhanek, D.L.; Oh, J.H.; Green, M.J. Radio frequency heating and reduction of graphene oxide and graphene oxide-polyvinyl alcohol composites. *Carbon* **2020**, *169*, 475–481. [[CrossRef](#)]
118. Shuai, C.; Feng, P.; Gao, C.; Shuai, X.; Xiao, T.; Peng, S. Graphene oxide reinforced poly(vinyl alcohol): Nanocomposite scaffolds for tissue engineering applications. *RSC Adv.* **2015**, *5*, 25416–25423. [[CrossRef](#)]
119. Wang, Y.; Shen, C.; Lou, W.; Shentu, F. Fiber optic humidity sensor based on the graphene oxide/PVA composite film. *Opt. Commun.* **2016**, *372*, 229–234. [[CrossRef](#)]
120. Syuhada, A.; Shamsudin, M.S.; Daud, S.; Krishnan, G.; Harun, S.W.; Aziz, M.S.A. Single-mode modified tapered fiber structure functionalized with GO–PVA composite layer for relative humidity sensing. *Photonic Sens.* **2021**, *11*, 314–324. [[CrossRef](#)]
121. Kaur, R.; Arora, A.; Tripathi, S.K. Fabrication and characterization of metal insulator semiconductor Ag/PVA/GO/PVA/n-Si/Ag device. *Microelectron. Eng.* **2020**, *233*, 111419. [[CrossRef](#)]
122. Hmar, J.J.L. Non-volatile resistive switching memory device based on ZnO-graphene oxide embedded in a polymer matrix fabricated on a flexible PET substrate. *Microelectron. Eng.* **2020**, *233*, 111436. [[CrossRef](#)]
123. Ngo, H.T.; Thi, M.T.N.; Do, D.P.; Tran, K.M.; Thi, K.H.T.; Phan, B.T.; Pham, K.N. Low operating voltage resistive random access memory based on graphene oxide—Polyvinyl alcohol nanocomposite thin films. *J. Sci. Adv. Mater. Devices* **2020**, *5*, 199–206. [[CrossRef](#)]
124. Hwang, S.; Kang, D.; Ruoff, R.S.; Shin, H.S.; Park, Y. Poly (vinyl alcohol) Reinforced and toughened with poly(dopamine)-treated graphene oxide, and its use for humidity. *ACS Nano* **2014**, *8*, 6739–6747. [[CrossRef](#)] [[PubMed](#)]
125. Trigona, C.; Al-hamry, A.; Kanoun, O.; Baglio, S. Hybrid micro electro mechanical sensor based on graphene oxide/polyvinyl alcohol for humidity. *Proceedings* **2018**, *2*, 1011.
126. Lim, M.; Shin, H.; Shin, D.M.; Lee, S.; Lee, J. Poly(vinyl alcohol) nanocomposites containing reduced graphene oxide coated with tannic acid for humidity sensor. *Polymer* **2016**, *84*, 89–98. [[CrossRef](#)]
127. Lee, M.E.; Jin, H. Nanocomposite films of poly(vinyl alcohol)-grafted graphene oxide/poly(vinyl alcohol) for gas barrier film applications. *J. Nanosci. Nanotechnol.* **2015**, *15*, 8348–8352. [[CrossRef](#)]
128. Omar, N.A.S.; Fen, Y.W.; Abdullah, J.; Kamil, Y.M.; Daniyal, W.M.E.M.M.; Sadrolhosseini, A.R.; Mahdi, M.A. Sensitive detection of dengue virus type 2 E-Proteins signals using self-assembled monolayers/reduced graphene oxide-PAMAM dendrimer thin film-SPR optical sensor. *Sci. Rep.* **2020**, *10*, 2374. [[CrossRef](#)]
129. Fen, Y.W.; Yunus, W.M.M.; Talib, Z.A.; Yusof, N.A. Development of surface plasmon resonance sensor for determining zinc ion using novel active nanolayers as probe. *Spectrochim. Acta Part A Mol. Biomol. Spectrosc.* **2015**, *134*, 48–52. [[CrossRef](#)]
130. Fen, Y.W.; Yunus, W.M.M. Utilization of chitosan-based sensor thin films for the detection of lead ion by surface plasmon resonance optical sensor. *IEEE Sens. J.* **2013**, *13*, 1413–1418. [[CrossRef](#)]
131. Ramdzan, N.S.M.; Fen, Y.W.; Omar, N.A.S.; Anas, N.A.A.; Daniyal, W.M.E.M.M.; Saleviter, S.; Zainudin, A.A. Optik Optical and surface plasmon resonance sensing properties for chitosan/carboxyl-functionalized graphene quantum dots thin film. *Optik* **2019**, *178*, 802–812. [[CrossRef](#)]
132. Fen, Y.W.; Yunus, W.M.M.; Yusof, N.A.; Ishak, N.S.; Omar, N.A.S.; Zainudin, A.A. Preparation, characterization and optical properties of ionophore doped chitosan biopolymer thin film and its potential application for sensing metal ion. *Optik* **2015**, *126*, 4688–4692. [[CrossRef](#)]
133. Fen, Y.W.; Yunus, W.M.M.; Moksini, M.M.; Talib, Z.A.; Yusof, N.A. Surface plasmon resonance optical sensor for mercury ion detection by crosslinked chitosan thin film. *J. Optoelectron. Adv. Mater.* **2011**, *13*, 279–285.
134. Zainuddin, N.H.; Fen, Y.W.; Alwahib, A.A.; Yaacob, M.H.; Bidin, N.; Omar, N.A.S.; Mahdi, M.A. Detection of adulterated honey by surface plasmon resonance optical sensor. *Optik* **2018**, *168*, 134–139. [[CrossRef](#)]

135. Eddin, F.B.K.; Fen, Y.W.; Omar, N.A.S.; Liew, J.Y.C.; Daniyal, W.M.E.M.M. Femtomolar detection of dopamine using surface plasmon resonance sensor based on chitosan/graphene quantum dots thin film. *Spectrochim. Acta Part A Mol. Biomol. Spectrosc.* **2021**, *263*, 120202. [[CrossRef](#)]
136. Omar, N.A.S.; Fen, Y.W.; Ramli, I.; Sadrolhosseini, A.R.; Abdullah, J.; Yusof, N.A.; Kamil, Y.M.; Mahdi, M.A. An optical sensor for dengue envelope proteins using polyamidoamine dendrimer biopolymer-based nanocomposite thin film: Enhanced sensitivity, selectivity, and recovery studies. *Polymers* **2021**, *13*, 762. [[CrossRef](#)]
137. Mitchell, J. Small molecule immunosensing using surface plasmon resonance. *Sensors* **2010**, *10*, 7323–7346. [[CrossRef](#)]
138. Fen, Y.W.; Yunus, W.M.M.; Yusof, N.A. Surface plasmon resonance optical sensor for detection of Pb²⁺ based on immobilized p-tert-butylcalix [4] arene-tetrakis in chitosan thin film as an active layer. *Sens. Actuators B Chem.* **2012**, *171–172*, 287–293. [[CrossRef](#)]
139. Fen, Y.W.; Yunus, W.M.M.; Talib, Z.A. Analysis of Pb (II) ion sensing by crosslinked chitosan thin film using surface plasmon resonance spectroscopy. *Opt.-Int. J. Light Electron. Opt.* **2013**, *124*, 126–133. [[CrossRef](#)]
140. Fen, Y.W.; Yunus, W.M.M. Surface plasmon resonance spectroscopy as an alternative for sensing heavy metal ions: A review. *Sens. Rev.* **2009**, *33*, 305–314.
141. Fen, Y.W.; Mahmood, W.; Yunus, M.; Yusof, N.A. Detection of mercury and copper ions using surface plasmon resonance optical sensor. *Sens. Mater.* **2011**, *23*, 325–334.
142. Zaid, M.H.M.; Matori, K.A.; Aziz, S.H.A.; Kamari, H.M.; Wahab, Z.A.; Fen, Y.W.; Alibe, I.M. Synthesis and characterization of low cost willemite based glass—Ceramic for opto-electronic applications. *J. Mater. Sci. Mater. Electron.* **2016**, *27*, 11158–11167. [[CrossRef](#)]
143. Daniyal, W.M.E.M.M.; Saleviter, S.; Fen, Y.W. Development of surface plasmon resonance spectroscopy for metal ion development of surface plasmon resonance spectroscopy for metal ion detection. *Sens. Mater.* **2018**, *30*, 2023–2028.
144. Fen, Y.W.; Yunus, W.M.M.; Yusof, N.A. Optical properties of cross-linked chitosan thin film for copper ion detection using surface plasmon resonance technique. *Opt. Appl.* **2011**, *41*, 999–1013.
145. Eddin, F.B.K.; Fen, Y.W. Recent advances in electrochemical and optical sensing of dopamine. *Sensors* **2020**, *20*, 1039. [[CrossRef](#)]
146. Ramdzan, N.S.M.; Fen, Y.W.; Anas, N.A.A.; Omar, N.A.S.; Saleviter, S. Development of biopolymer and conducting polymer-based optical sensors for heavy metal ion detection. *Molecules* **2020**, *25*, 2548. [[CrossRef](#)]
147. Roshidi, M.D.A.; Fen, Y.W.; Daniyal, W.M.E.M.M.; Omar, N.A.S.; Zulholinda, M. Structural and optical properties of chitosan—Poly(amidoamine) dendrimer composite thin film for potential sensing Pb²⁺ using an optical spectroscopy. *Opt.-Int. J. Light Electron. Opt.* **2019**, *185*, 351–358. [[CrossRef](#)]
148. Eddin, F.B.K.; Fen, Y.W. The principle of nanomaterials based surface plasmon resonance biosensors and its potential for dopamine detection. *Molecules* **2020**, *25*, 2769. [[CrossRef](#)]
149. Fauzi, N.I.M.; Fen, Y.W.; Omar, N.A.S.; Saleviter, S.; Daniyal, W.M.E.M.M.; Hashim, H.S.; Nasrullah, M. Nanostructured chitosan/maghemite composites thin film for potential optical detection of mercury ion by surface plasmon resonance investigation. *Polymers* **2020**, *12*, 1497. [[CrossRef](#)]
150. Daniyal, W.M.E.M.M.; Fen, Y.W.; Fauzi, N.I.M.; Hashim, H.S.; Ramdzan, N.S.; Omar, N.A.S. Recent advances in surface plasmon resonance optical sensors for potential application in environmental monitoring. *Sens. Mater.* **2020**, *32*, 4191–4200. [[CrossRef](#)]
151. Daniyal, W.M.E.M.M.; Fen, Y.W.; Abdullah, J.; Sadrolhosseini, A.R.; Saleviter, S.; Omar, N.A.S. Exploration of surface plasmon resonance for sensing copper ion based on nanocrystalline cellulose-modified thin film. *Opt. Express* **2018**, *26*, 34880–34893. [[CrossRef](#)] [[PubMed](#)]
152. Saleviter, S.; Fen, Y.W.; Daniyal, W.M.E.M.M.; Abdullah, J.; Sadrolhosseini, A.R.; Omar, N.A.S. Design and analysis of surface plasmon resonance optical sensor for determining cobalt ion based on chitosan-graphene oxide decorated quantum dots-modified gold active layer. *Opt. Express* **2019**, *27*, 32294–32307. [[CrossRef](#)] [[PubMed](#)]
153. Anas, N.A.A.; Fen, Y.W.; Yusof, N.A.; Omar, N.A.S.O.; Daniyal, W.M.E.M.M.; Ramdzan, N.S.M. Highly sensitive surface plasmon resonance optical detection of ferric ion using CTAB/hydroxylated graphene quantum dots thin film. *J. Appl. Phys.* **2020**, *128*, 83105. [[CrossRef](#)]
154. Omar, N.A.S.; Fen, Y.W.; Abdullah, J.; Zaid, M.H.M.; Mahdi, M.A. Structural, optical and sensing properties of CdS-NH₂GO thin film as a dengue virus E-protein sensing material. *Opt.-Int. J. Light Electron. Opt.* **2018**, *171*, 934–940. [[CrossRef](#)]
155. Hashim, H.S.; Fen, Y.W.; Omar, N.A.S.; Daniyal, W.M.E.M.M.; Saleviter, S.; Abdullah, J. Structural, optical and potential sensing properties of tyrosinase immobilized graphene oxide thin film on gold surface. *Opt.-Int. J. Light Electron. Opt.* **2020**, *212*, 164786. [[CrossRef](#)]
156. Ramdzan, N.S.M.; Fen, Y.W.; Omar, N.A.S.; Anas, N.A.A.; Liew, J.Y.C.; Daniyal, W.M.E.M.M.; Hashim, H.S. Detection of mercury ion using surface plasmon resonance spectroscopy based on nanocrystalline cellulose/poly(3,4-ethylenedioxythiophene) thin film. *Measurement* **2021**, *182*, 109728. [[CrossRef](#)]
157. Bao, C.; Guo, Y.; Song, L.; Hu, Y. Poly(vinyl alcohol) nanocomposites based on graphene and graphite oxide: A comparative investigation of property and mechanism. *Chem. J. Mater.* **2011**, *21*, 13942–13950. [[CrossRef](#)]
158. Yang, X.; Li, L.; Shang, S.; Tao, X. Synthesis and characterization of layer-aligned poly(vinyl alcohol)/graphene nanocomposites. *Polymer* **2010**, *51*, 3431–3435. [[CrossRef](#)]

159. Islam, M.R. Enhanced electrochemical performance of solution-processed single-wall carbon nanotube reinforced polyvinyl alcohol nanocomposite synthesized via solution-cast method Enhanced electrochemical performance of solution-processed single-wall carbon nanotube. *Nano Express* **2020**, *1*, 30013. [[CrossRef](#)]
160. Yahia, I.S.; Mohammed, M.I. Facile synthesis of graphene oxide/PVA nanocomposites for laser optical limiting: Band gap analysis and dielectric constants. *J. Mater. Sci. Mater. Electron.* **2018**, *29*, 8555–8563. [[CrossRef](#)]
161. Wu, T.; Chen, B. Facile fabrication of porous conductive thermoplastic polyurethane nanocomposite films via solution casting. *Sci. Rep.* **2017**, *7*, 17470. [[CrossRef](#)] [[PubMed](#)]
162. Islam, M.R.; Mollik, I. Enhanced electrochemical performance of flexible and eco-friendly starch/graphene oxide nanocomposite. *Heliyon* **2020**, *6*, e05292. [[CrossRef](#)] [[PubMed](#)]
163. Mo, S.; Peng, L.; Yuan, C.; Zhao, C.; Tang, W.; Ma, C.; Shen, J.; Yang, W.; Yu, Y.; Min, Y.; et al. Enhanced properties of poly(vinyl alcohol) composite films with functionalized graphene. *RSC Adv.* **2015**, *5*, 97738–97745. [[CrossRef](#)]
164. Omar, N.A.S.; Irmawati, R.; Fen, Y.W.; Muhamad, E.N.; Eddin, F.B.K.; Anas, N.A.A.; Ramdhan, N.S.M.; Fauzi, N.I.M.; Mahdi, M.A. Surface refractive index sensor based on titanium dioxide composite thin film for detection of cadmium ions. *Measurement* **2021**, *187*, 110287. [[CrossRef](#)]
165. Xie, M.; Zhao, F.; Zhang, Y.; Xiong, Y.; Han, S. Recent advances in aptamer-based optical and electrochemical biosensors for detection of pesticides and veterinary drugs. *Food Control* **2022**, *131*, 108399. [[CrossRef](#)]
166. Gong, C.; Fan, Y.; Zhao, H. Recent advances and perspectives of enzyme-based optical biosensing for organophosphorus pesticides detection. *Talanta* **2022**, *240*, 123145. [[CrossRef](#)]
167. Wang, Y.; Zhang, X.; Zhang, X.; Zhou, T.; Cui, Z.; Zhang, K. A novel terahertz metasurface based on a single-walled carbon nanotube film for sensing application. *J. Mater. Chem. A* **2022**, *10*, 1780–1787. [[CrossRef](#)]
168. Byrne, B.; Stack, E.; Gilmartin, N.; O’Kennedy, R. Antibody-based sensors: Principles, problems and potential for detection of pathogens and associated toxins. *Sensors* **2009**, *9*, 4407–4445. [[CrossRef](#)]
169. Ramdhan, N.S.M.; Fen, Y.W.; Liew, J.Y.C.; Omar, N.A.S.; Anas, N.A.A.; Daniyal, W.M.E.M.M.; Fauzi, I.M.F. Exploration on structural and optical properties of nanocrystalline cellulose/poly(3,4-ethylenedioxythiophene) thin film for potential plasmonic sensing application. *Photonics* **2021**, *8*, 419. [[CrossRef](#)]
170. Sun, Z.; Cui, Z.; Li, H. p-Amino benzenesulfonic acid functionalized gold nanoparticles: Synthesis, colorimetric detection of carbaryl and mechanism study by zeta potential assays. *Sens. Actuators B Chem.* **2013**, *183*, 297–302. [[CrossRef](#)]
171. Tsagkaris, A.S.; Uttl, L.; Pulkrabova, J.; Hajslova, J. Screening of carbamate and organophosphate pesticides in food matrices using an affordable and simple spectrophotometric acetylcholinesterase assay. *Appl. Sci.* **2020**, *10*, 565. [[CrossRef](#)]
172. Zhang, Y.; Gao, L.; Ma, S.; Hu, T. Porous MB@Cd-MOF Obtained by Post-Modification: Self-Calibrated Fluorescent Turn-on Sensor for Highly Sensitive Detection of carbaryl. *Cryst. Growth Des.* **2022**, *22*, 2662–2669. [[CrossRef](#)]
173. Hossain, S.Z.; Luckham, R.E.; McFadden, M.J.; Brennan, J.D. Reagentless bidirectional lateral flow bioactive paper sensors for detection of pesticides in beverage and food samples. *Anal. Chem.* **2009**, *81*, 9055–9064. [[CrossRef](#)] [[PubMed](#)]
174. Minh, P.N.; Hoang, V.; Dinh, N.X.; Hoang, O.V.; Cuong, N.V.; Hop, D.T.B.; Tuan, T.Q.; Khi, N.T.; Huy, T.Q.; Le, A. Reduced graphene oxide-wrapped silver nanoparticles for applications to ultrasensitive colorimetric detection of Cr (VI) ions and carbaryl pesticide. *New J. Chem.* **2020**, *44*, 7611–7620. [[CrossRef](#)]
175. Mauriz, E.; Calle, A.; Manclus, J.J.; Montoya, A.; Escuela, A.M.; Sendra, J.R.; Lechuga, L.M. Single and multi-analyte surface plasmon resonance assays for simultaneous detection of cholinesterase inhibiting pesticides. *Sens. Actuators B* **2006**, *118*, 399–407. [[CrossRef](#)]
176. Mauriz, E.; Calle, A.; Lechuga, L.M.; Quintana, J.; Montoya, A.; Mancl, J.J. Real-time detection of chlorpyrifos at part per trillion levels in ground, surface and drinking water samples by a portable surface plasmon resonance immunosensor. *Anal. Chim. Acta* **2006**, *561*, 40–47. [[CrossRef](#)]
177. Chen, J.; Liu, Z.; Fang, J.; Wang, Y.; Cao, Y.; Xu, W.; Ma, Y.; Meng, X.; Wang, B. A turn-on fluorescence biosensor for sensitive detection of carbaryl using flavourzyme-stabilized gold nanoclusters. *LWT* **2022**, *157*, 113099. [[CrossRef](#)]
178. Soriano, M.L.; Jimenez-Sanchez, A.; Cardenas, S. Passivated graphene quantum dots for carbaryl determination in juices. *J. Sep. Sci.* **2021**, *44*, 1652–1661. [[CrossRef](#)]
179. Chen, Y.; Qin, X.; Yuan, C.; Shi, R.; Wang, Y. Double responsive analysis of carbaryl pesticide based on carbon quantum dots and Au nanoparticles. *Dyes Pigm.* **2020**, *181*, 108529. [[CrossRef](#)]
180. Shahdost-fard, F.; Fahimi-Kashani, N.; Hormozi-nezhad, M.R. A ratiometric fluorescence nanoprobe using CdTe QDs for fast detection of carbaryl insecticide in apple. *Talanta* **2020**, *221*, 121467. [[CrossRef](#)]
181. Cervera-chiner, L.; March, C.; Arnau, A. Detection of DDT and carbaryl pesticides in honey by means of immunosensors based on High Fundamental Frequency Quartz Crystal Microbalance (HFF-QCM). *J. Sci. Food Agric.* **2020**, *100*, 2468–2472. [[CrossRef](#)] [[PubMed](#)]
182. Zhang, C.; Cui, H.; Cai, J.; Duan, Y.; Liu, Y. Development of fluorescence sensing material based on cdse/zns quantum dots and molecularly imprinted polymer for the detection of carbaryl in rice and chinese cabbage. *J. Agric. Food Chem.* **2015**, *63*, 5–11. [[CrossRef](#)] [[PubMed](#)]